The antiferroelectric-ferroelectric-paraelectric phase sequence in lead-lanthanum zirconate-titanate ceramics with 8% Ti content

1994 J. Phys.: Condens. Matter 6 6843

(http://iopscience.iop.org/0953-8984/6/34/016)

J. Phys.: Condens. Matter 6 (1994) 6843–6856. Printed in the UK

The antiferroelectric–ferroelectric–paraelectric phase sequence in lead–lanthanum zirconate–titanate ceramics with 8% Ti content

Z Ujma†, J Handerek†, M Pawełczyk†, H Hassan‡, G E Kugel‡ and C Carabatos-Nedelec‡

† Institute of Physics, Silesian University, 40-007 Katowice, ul. Uniwersytecka 4, Poland
‡ Centre Lorrain d'Optique et Electronique des Solides, Université de Metz, 2 Belin, 570078 Metz Cédex 3, France

Received 7 March 1994, in final form 4 May 1994

Abstract. Phase transitions in PLZT 2/92/8 ceramics were investigated by x-ray, dielectric, pyroelectric and Raman scattering measurements. The antiferroelectric–ferroelectric–paraelectric phase sequence in this material was confirmed. The antiferroelectric and ferroelectric phases coexist in an exceptionally wide low-temperature range. Possible reasons for the differentiation in properties of the ferroelectric phase in the high- and low-temperature ranges are discussed.

1. Introduction

The ferroelectric-paraelectric phase sequence with low- and high-temperature ferroelectric phases of rhombohedral symmetry ($F_{R(LT)}$, $R3c$; $F_{R(HT)}$, $R3m$) have most often been ascertained in Zr-rich $Pb(Zr_xTi_{1-x})O_3$ (PZT) and $(Pb_yLa_{1-y})(Zr_xTi_{1-x})O_3$ (PLZT) solid solutions with $0.52 < x < 0.94$–0.95 [1–11] (figure 1). These solutions with $0.94 < x < 1.0$ also show a transition to the antiferroelectric phase of orthorhombic symmetry (A_O, $Pbam$). Certain indications of the F_R–A_O phase transition were also observed in PZT and PLZT ceramics with Ti contents of 8% and 10% [12, 13]. Observed changes in the intensity of chosen lines in the Raman spectra and the appearance of certain additional modes may be attributed to doubling of the unit cell during the $F_{R(HT)}$–$F_{R(LT)}$ transition [14–16] but they can also be attributed to the transition to the A_O phase [12]. The $F_{R(LT)}$–$F_{R(HT)}$ transition has been relatively little studied for PZT and PLZT ceramics with a Zr/Ti ratio close to 94/6 owing to the virtually undetectable anomalies in the dielectric and other characteristics of these ceramics. Close to Zr/Ti= 94/6, the phase boundary separating F_R and A_O phases (figure 1) is not steep as many workers suggest. Certain data given in the literature on PZT and PLZT solutions close to this boundary raise doubts whether such ceramics, even with slightly greater Ti contents show both $F_{R(HT)}$–$F_{R(LT)}$ and $F_{R(LT)}$–A_O transitions or only one of them.

We have reported results of structural, dielectric and pyroelectric investigations and of Raman spectroscopy investigations for PLZT and Nb-doped PZT ceramics with a Zr/Ti ratio of 95/5 in earlier papers [11, 17–20]. Given here are the results of similar investigations for PLZT ceramics with La/Zr/Ti ratios of 2/92/8, where the first number means 2 mol% of La_2O_3 (i.e. 4 atom% of La in the Pb sublattice). In this case, investigations were extended towards the low-temperature region, which has been much less studied up to now. The

0953-8984/94/346843+14$19.50

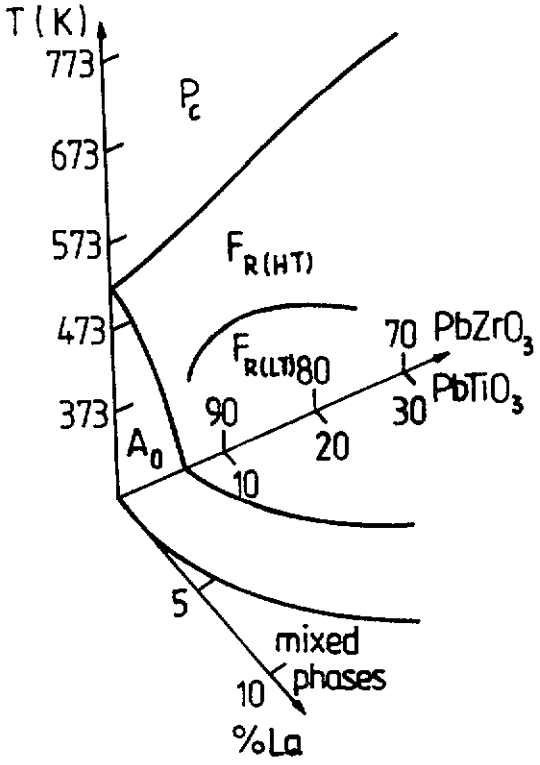

Figure 1. Zr-rich part of the PZT and PLZT phase diagrams (according to [23]).

results obtained provide the basis for a wider discussion of the F_R–A_O phase transition and the coexistence of these phases, observed in a wide low-temperature range.

2. X-ray investigations

The PLZT 2/92/8 ceramics were prepared using the conventional method of thermal synthesis of mixed PbO, ZrO_2, TiO_2 and La_2O_3 in suitable proportions. The final sintering was performed at 1523 K for 12 h in a double crucible with a PbO atmosphere, ensuring that the established composition was maintained. Owing to the low porosity the ceramics obtained are partially transparent, i.e. about 30% transparency in the visible range of light for a sample 1 mm thick.

A disc sample of diameter 17 mm and thickness 1 mm was used for x-ray measurements. Measurements were performed on a modified DRON diffractometer with suitable low- and high-temperature attachments, permitting temperature stabilization with an accuracy of ± 0.5 K. Measurements were carried out during the cooling and heating processes in the temperature ranges below and above room temperature, respectively.

Cu Kα radiation was used for phase analysis and to determine the pseudo-perovskite cell parameters. To determine the F_R and A_O phase contents the {222} and {200} reflections were considered because of their characteristic multiplet shape in the particular phases. Variation in the intensity of reflections associated with the F_R and A_O phases in the vicinities of the F_R–P_C and F_R–A_O phase transitions was assumed to be proportional to the contents of

these phases in the sample. The numerical method was used to separate partly overlapping reflections, and to obtain the integrated intensities of the diffraction lines. The relative changes in these intensities were taken to be a measure of the content of the separate phases. Using this procedure the temperature dependences of the F_R and A_O phase contents were obtained independently (figure 2). The content of the regular P_C phase was calculated as the complement of the 100% ferroelectric F_R phase content. There are regions in which the neighbouring phases coexist. The points at which the volume content of the coexisting phases is the same correspond to the average T_{F-P} and T_{F-A} phase transition temperatures. It is noteworthy that the F_R–A_O phase transition is exceptionally diffuse.

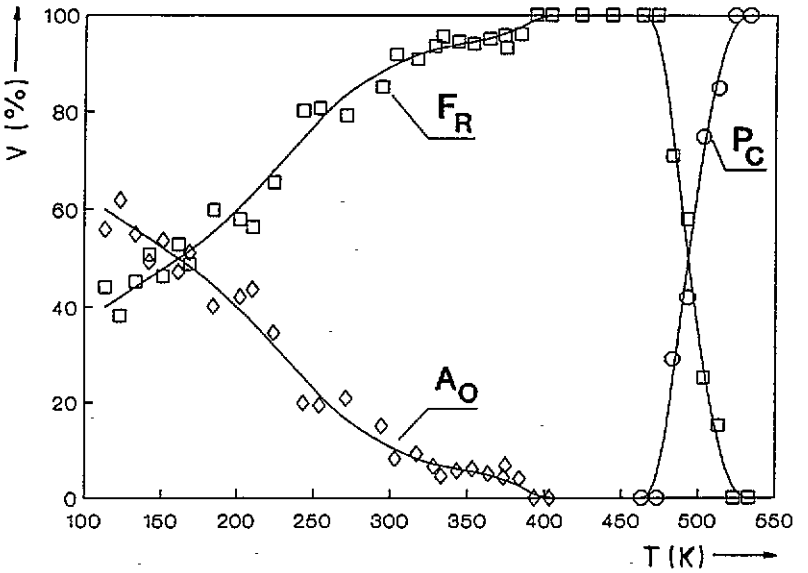

Figure 2. Percentage content of the P_C, F_R and A_O phases versus temperature.

The temperature dependences of the pseudo-perovskite cell parameters are shown in figure 3. Only the F_R–P_C and F_R–A_O phase transitions are indicated by these data. We did not observe separate diffraction lines or other changes in characteristics shown in figures 2 and 3, which could be indicative of an $F_{R(HT)}$–$F_{R(LT)}$ transition.

3. Dielectric and pyroelectric measurements

A sample of 0.6 mm thickness with deposited silver electrodes was used for measurements of the electric permittivity ϵ and dissipation factor $\tan\delta$ as functions of temperature. These measurements were performed at chosen frequencies of measuring field in the range 0.1–20 kHz using a computerized automatic measuring system based on a Tesla BM-595 RLCG meter. The $\epsilon(T)$ and $\tan\delta(T)$ curves on heating are shown in figures 4 and 5. At the F_R–P_C phase transition temperature, sharp maxima occur in the $\epsilon(T)$ curves. The local maxima and local minima in the $\tan\delta(T)$ curves occur below T_{F-P}, and in the vicinity of this temperature, respectively. The temperatures at which these minima occur increase with

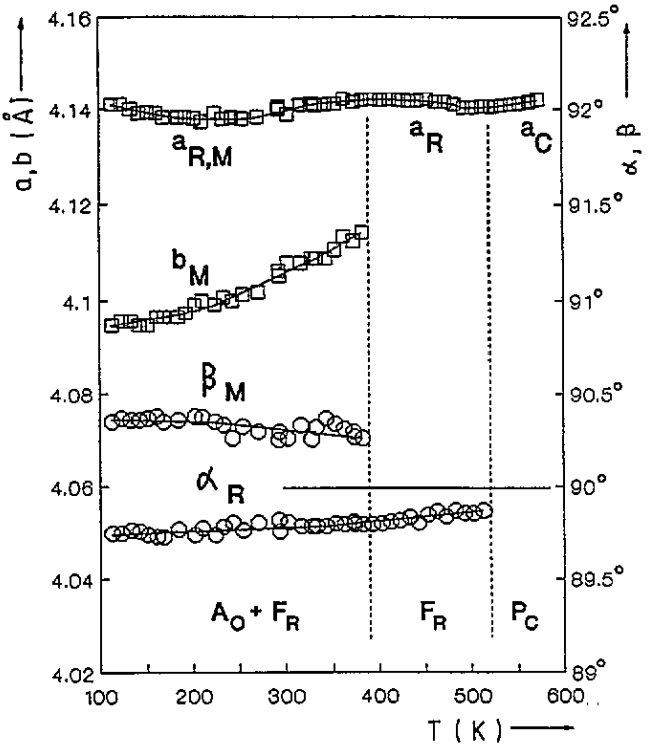

Figure 3. Pseudo-perovskite unit-cell parameters as a function of temperature: a_C, a_R, b_M, edges of the pseudo-perovskite cell in the cubic, rhombohedral and monoclinic phases, respectively; $a_{R,M}$, edge of the pseudo-perovskite cell common to rhombohedral and monoclinic phases; α_R, rhombohedral angle between a_R edges; β_M, monoclinic angle between a_M edges.

increasing frequency of the measuring field. At high temperatures in the paraelectric phase range, additional broadened maxima in the $\epsilon(T)$ curves and associated anomalies in the $\tan\delta(T)$ curves are found and are more distinct for low frequencies.

In the temperature range in which the F_R and A_O phases coexist the $\epsilon(T)$ curves show only insignificant anomalies even in the vicinity of the markedly broadened F_R–A_O phase transition (see figures 2 and 4), while strong thermal hysteresis is found in the $\epsilon(T)$ curves. Much more distinct changes in the $\tan\delta(T)$ curves occur in the temperature range where the F_R and A_O phases coexist where there is an increase in $\tan\delta(T)$ in a wide temperature range (figure 5).

Remanent polarization P_r as a function of temperature was obtained from measurements of the hysteresis loop in a field of frequency 50 Hz and strength 10 kV cm^{-1}. The remanent polarization obtained in this way and also the coercive field E_C as functions of temperature are shown in figure 6 for the heating and cooling processes. Deviations from the linear $P(E)$ dependence and slim hysteresis loops were first observed during heating when passing through the temperature range in which the A_O phase residue disappears (see figure 2). With further increase in temperature they gradually transform to normal hysteresis loops. A steep increase in the $P_r(T)$ curves and linear decrease in the $E_C(T)$ curves takes place in this temperature range. The hysteresis loops and $P_r(T)$ exhibit nearly classical behaviour in the vicinity of the F_R–P_C phase transitions. A steep decrease in P_r-values was observed while passing through a temperature of about 380 K in cooling, while x-ray measurements showed

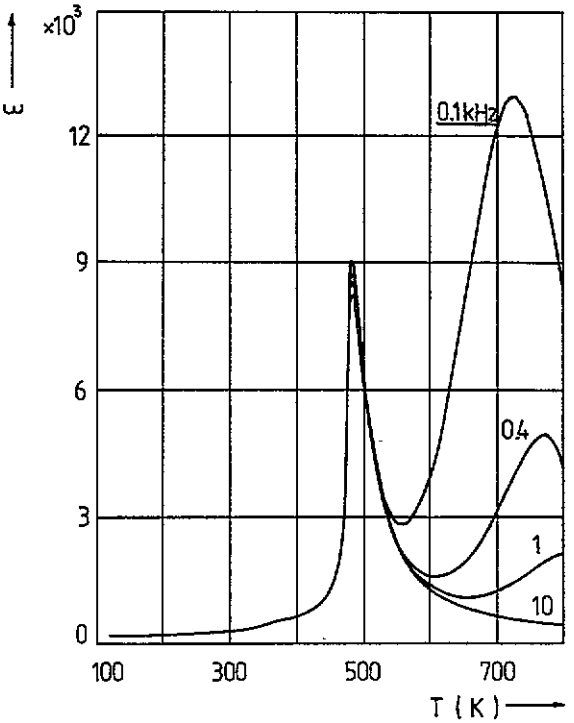

Figure 4. Temperature dependence of the permittivity, measured at the chosen frequencies of the measuring field, on heating.

the presence of the A_O phase in a predominantly F_R-phase matrix (figure 2). The $P_r(T)$ curves showed an exceptionally large thermal hysteresis (about 50 K) in this temperature range.

Prior to pyroelectric measurements the sample was pre-polarized for 0.5 h at a temperature of 543 K in a DC field of 5 kV cm^{-1} strength and then cooled in this field to 100 K. The thermally stimulated depolarization current (TSDC) recorded during subsequent heating at 5 K min^{-1} is shown in figure 7. A steep peak of the pyroelectric current on the TSDC background appeared in the vicinity of the F_R–P_C phase transition temperature. A wide TSDC peak was then observed in the paraelectric phase with a maximum at about 600 K. This current curve showed an activated form in the temperature range below its maximum. There is clear correlation between the behaviour of this current and the wide maxima in the $\epsilon(T)$ curves and the extrema in the $\tan\delta(T)$ curves observed in the same temperature range.

No pyroelectric current associated with the changes in $P_r(T)$ curves was observed in the temperature range about 320–420 K (figure 6). Hence it is evident that these changes in the $P_r(T)$ curves are not caused by the abrupt appearance or disappearance of the F_R phase but by some other processes, only partially associated with the F_R–A_O phase transition.

4. Raman scattering measurements

Raman scattering measurements were carried out on a SPEX double monochromator with an He–Ne laser (λ = 6328 Å) using a photon-counting read-out system and controlled

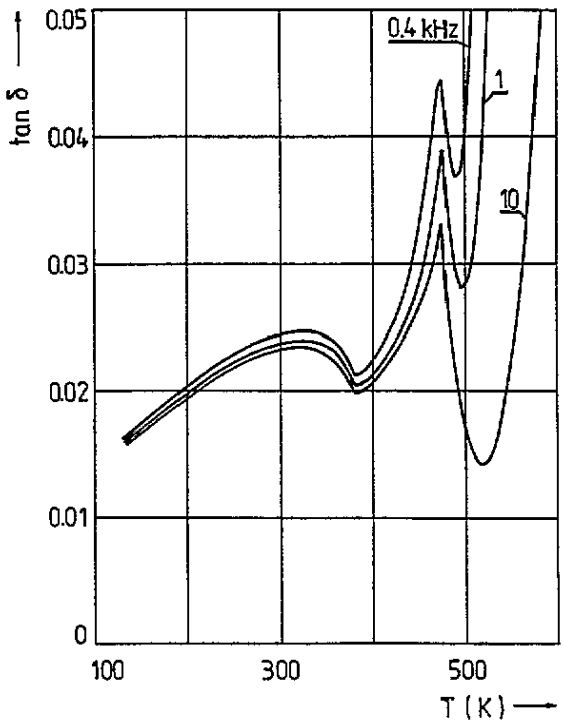

Figure 5. Temperature dependence of tan δ, measured at the chosen frequencies of the measuring field, on heating.

by the Datamate acquisition processor. The low-temperature spectra were recorded on a sample cooled in an Air Product Displex cryostat. Because of their low porosity, the PLZT 2/92/8 ceramics exhibit relatively high transparency and are suitable for use in 90°-geometry Raman scattering measurements. The Raman spectra were recorded in a wide temperature range extending from 10 to 700 K and in a frequency range covering the entire vibrational spectrum of the system. Since the experiments were performed on unpoled ceramics, no study as a function of laser light polarization was done and the spectra are consequently unpolarized.

Figure 8 shows the Raman spectra recorded at 10 K for PLZT 2/92/8 and PLZT 2/95/5 ceramics. In comparison with equivalent spectra recorded for pure $PbZrO_3$ single crystals [18, 19, 21] it is noteworthy that both the Raman spectra exhibit vibrational structures which are typical of the low-temperature antiferroelectric A_O phase which has been clearly ascertained in pure $PbZrO_3$ and in PZT 95/5. Nevertheless, certain important differences between these two spectra are apparent. In PLZT 2/92/8, well resolved structures are additionally detected at 23, 88 and 120 cm^{-1}.

Figure 9 presents typical Raman spectra recorded below room temperature in a cooling and heating process. Below 150 K the spectra observed in both processes are the same; significant differences arise in the scattered intensities in the temperature range between 200 and 300 K. These results appear to indicate a hysteresis effect which could follow after a low-temperature structural phase transition (figure 2).

Figure 10 shows Raman spectra recorded between room temperature and 613 K. On heating, the spectra are progressively modified in the sense that the low-frequency structure

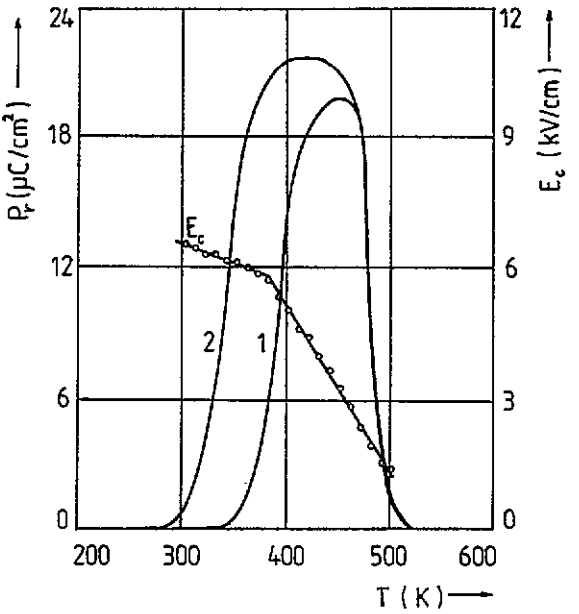

Figure 6. The remanent polarization obtained from hysteresis loop on heating (curve 1) and on cooling (curve 2) and the coercive field as functions of temperature.

increases their damping constant and leads to a signal described by quasi-elastic-type scattering accompanied by a broad overdamped low-frequency structure which is still visible in the paraelectric phase.

The shifts in the mode frequencies and dampings were analysed by performing systematic fits of the Raman profiles to response functions including a Debye-like function for the quasi-elastic scattering and Lorentzian functions for the resonant phonon scattering. Figure 11 presents the deduced temperature dependence of the squared Raman frequency in the frequency range up to 150 cm^{-1} and for temperatures up to 400 K. These data refer to the heating process. It may be seen that the low-frequency lines at 23, 36 and 53 cm^{-1} do not significantly change their frequencies with increasing temperature. The lines at 61 and 144 cm^{-1} shift slowly to lower frequencies with a singularity in the 200–250 K range which corresponds approximately to the average phase transition temperature between A_O and F_R found from x-ray analysis (figure 2). On the other hand, the lines at 80 and 120 cm^{-1} exhibit marked softening which can be clearly traced up to room temperature and which could be extrapolated to the high-temperature F_R–P_C transition [12]. Above this temperature their dampings strongly increase, leading to coalescence with neighbouring structures and consequent difficulty in resolution.

For such reasons and because of the complexity of the spectrum, accurate determination of all the phonon parameters (frequency, damping and scattering intensity) is particularly difficult, even in the low-frequency range. In order to gain a qualitative view of the constant-frequency light scattering intensity, a temperature dependence was plotted for the intensity scattered at 52 cm^{-1} which corresponds to the room-temperature position of one important line. The result is shown in figure 12 which indicates a small drop at about 200 K, followed by a considerable increase between 200 and 400 K and next a local anomaly at about 480 K followed by a gradual decrease after 530 K. About this last experiment it is worth noting that

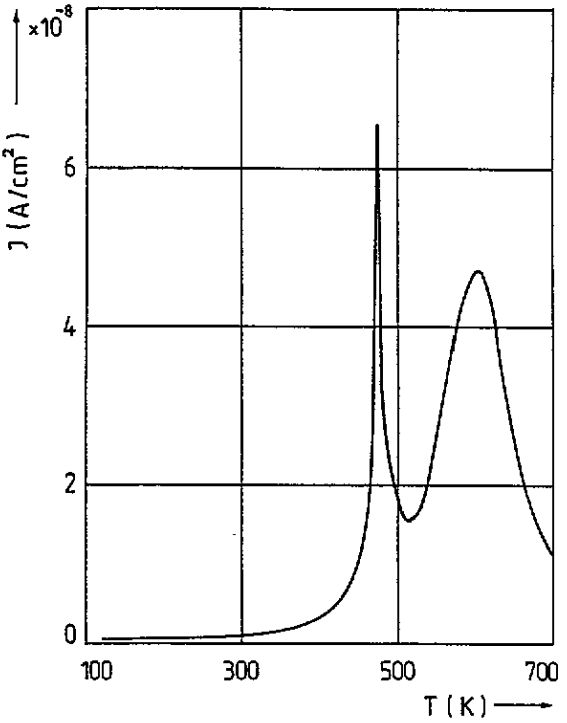

Figure 7. TSDC and pyroelectric current recorded on heating.

these results must be considered as qualitative since they were obtained dynamically with respect to temperature, without reaching complete thermodynamic equilibrium and since the measured intensity at this frequency (52 cm^{-1}) contains several scattering contributions. Simultaneously, when considered together with the TDSC (figure 7) and dielectric (figures 4 and 5) results, our light scattering data confirm the occurrence of an F_R–P_C phase transition.

5. Discussion

It is interesting to note the distinct similarities between the main structural, dielectric and spectroscopic characteristics of PLZT 2/92/8 ceramics reported here, and those of PZT and PLZT ceramics with Ti contents up to 5% [8, 11, 17–20] which we studied earlier and even for pure $PbZrO_3$ crystals [21]. All these materials exhibit an antiferroelectric–ferroelectric–paraelectric phase sequence. The fact that PLZT 2/92/8 ceramics also show this phase sequence was proved directly by x-ray measurements (figures 2 and 3). In this case, however, the A_O–F_R phase transition is exceptionally diffuse and the average temperature of this transition is strongly shifted towards lower temperatures, compared with the other materials mentioned. The similarity between all these materials is also apparent from comparison of their Raman spectra and their temperature evolution (figures 8–10). The low-temperature Raman spectra for PLZT 2/92/8 ceramics are, for the main peaks, clearly similar to typical spectra for orthorhombic antiferroelectric $PbZrO_3$ and solid solutions of PZT or PLZT with less than 6% Ti content [17–21]. The F_R phase, which appears on heating,

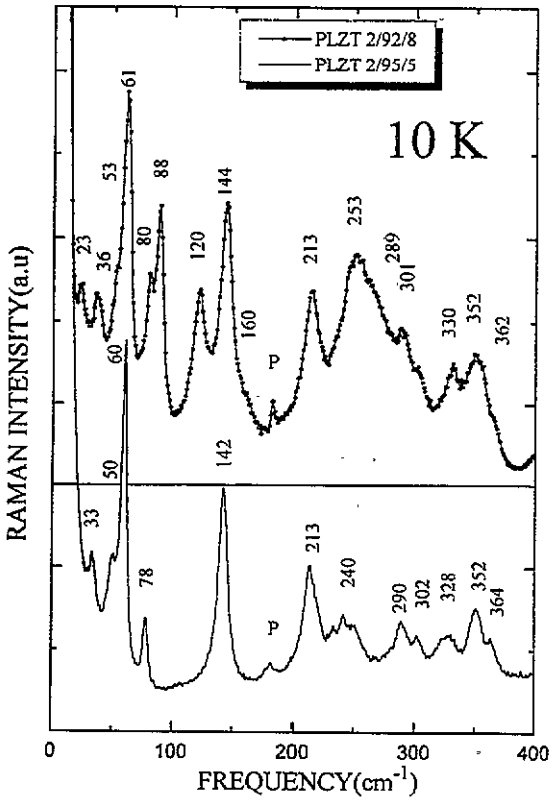

Figure 8. Comparison of the Raman spectra recorded at 10 K for PLZT 2/92/8 and for PLZT 2/95/5. The peak positions indicated for 10 K are used to determine the vibrational structure.

is associated with a steep increase in the light scattering mainly in the vicinity of the central peak (figure 12).

The similarity observable in the dielectric characteristics is more limited. These characteristics behave alike in the vicinity of the F_R–P_C phase transition and in the paraelectric phase. In the temperature range in which the F_R and A_O phases coexist, the dielectric characteristics show substantial differences, i.e. the typical hunch-like anomalies observed in the $\epsilon(T)$ curves, associated with a more or less broadened F_R–A_O phase transition [11], were insignificant. In the case of ceramics with a Ti content below 6%, a distinct correlation between $P_r(T)$ and anomalies in $\epsilon(T)$ characteristics was observed. However, in the case of PLZT 2/92/8 ceramics such a correlation was not confirmed from the F_R–A_O transition side. A striking fact is that the pyroelectric current associated with steep $P_r(T)$ changes on this side was not observed. Hence it may be concluded that, despite the similarity of the $P_R(T)$ dependences for PLZT and PZT ceramics with Ti contents greater and smaller than the critical value of 6%, the cause of such changes in $P_r(T)$ curves for PLZT 2/92/8 ceramics must be quite different. The specific features of the behaviours of these ceramics in this temperature range result, presumably, from the A_O phase occurring in the F_R matrix and from the very strongly diffuse character of the A_O–F_R phase transition. This latter is caused by large variations in the local A_O–F_R phase transition temperatures due to compositional fluctuations in the concentrations of Ti, Zr, Pb and La ions and vacancies in

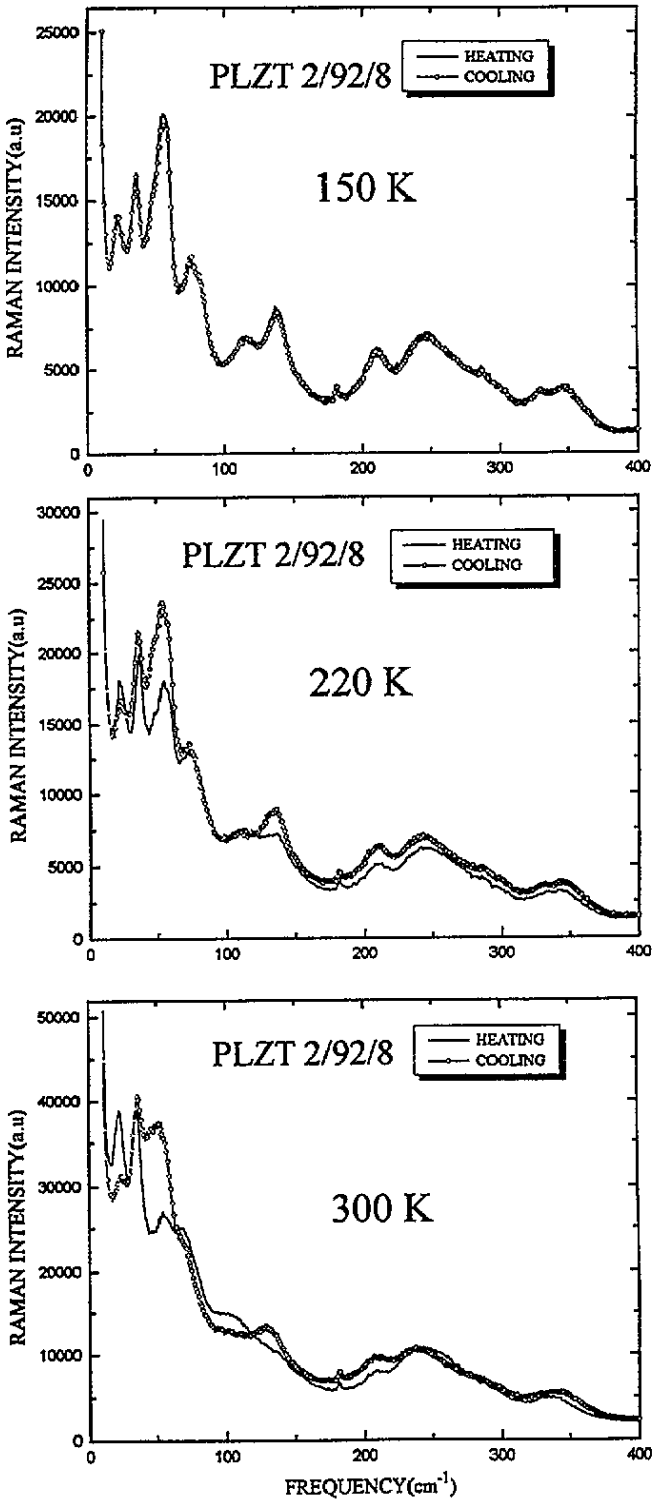

Figure 9. Temperature dependence of the low-frequency Raman spectra recorded for PLZT 2/92/8 at 150, 220 and 300 K in a heating and a cooling process.

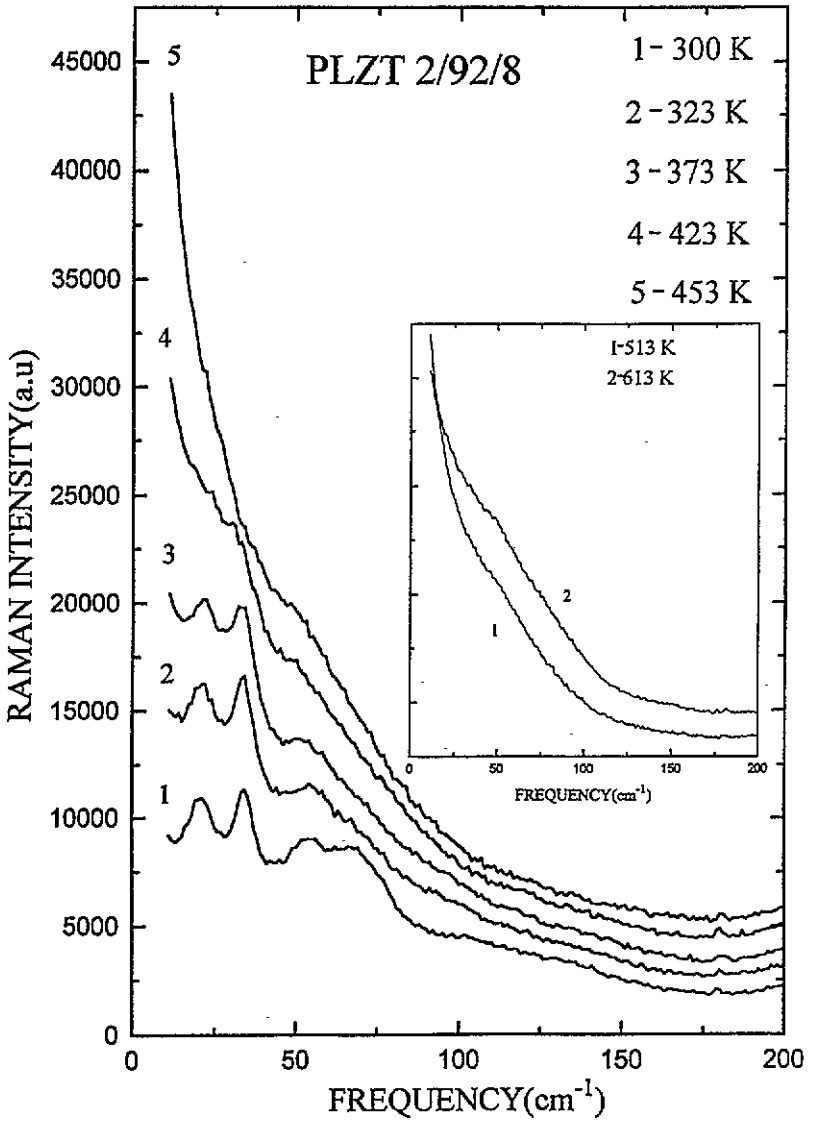

Figure 10. Temperature dependence of the Raman spectra recorded for PLZT 2/92/8 above room temperature.

the Pb and O sublattices and also to differing local electric fields and mechanical tensions. When the ferroelectric state disappears in the surroundings of some ferroelectric domain, the energy associated with its depolarization field must be minimalized locally by one of two possible compensation methods, known from macroscopic considerations. One of them involves the formation of the compensated polydomain structure, and especially twin domain formation. This latter has been found in PZT ceramics with Zr/Ti ratios of both 95/5 [22] and 90/10 [16]. This process plays a role in serving the ferroelectric domains in smaller and smaller microdomains, and finally in forming the antiferroelectric state. The second way involves P_s screening by the ion and electron space charges from the surrounding space or from electrodes. These remaining ferroelectric domains are stabilized in this way in the

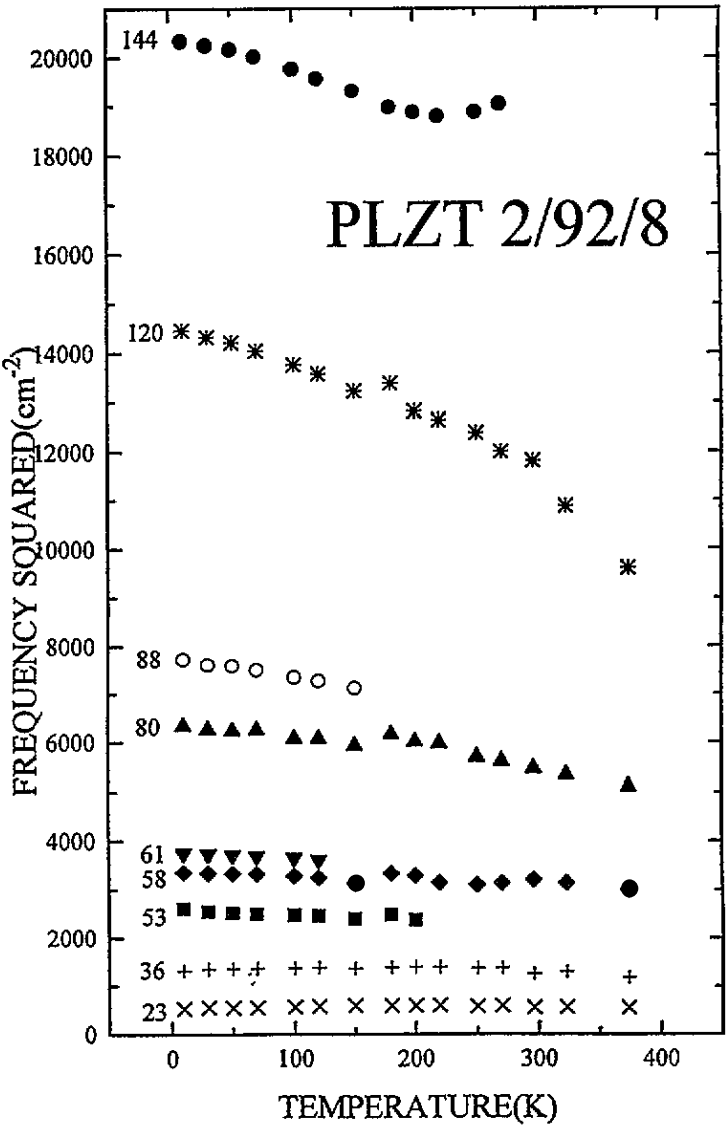

Figure 11. Temperature dependence of the squared frequency of the vibrational modes located below 150 cm^{-1} for the PLZT 2/92/8 ceramics.

antiferroelectric matrix. The P_s of such domains is not reversible and does not give rise to remanent polarization measured from the hysteresis loop. This could explain the gradual disappearance of the hysteresis loop on cooling below about 380 K (figure 6) despite the fact that the F_R phase still predominates even at much lower temperatures (figure 2). The release of the electron charges participating in the screening process can explain the $P_r(T)$ curve behaviour on heating.

It is noteworthy that none of the investigated structural, dielectric and spectral characteristics showed any clear indications of the $F_{R(HT)}$–$F_{R(LT)}$ phase transition in PZT or PLZT ceramics with Ti content greater than 6% (figure 1) mentioned in the introduction.

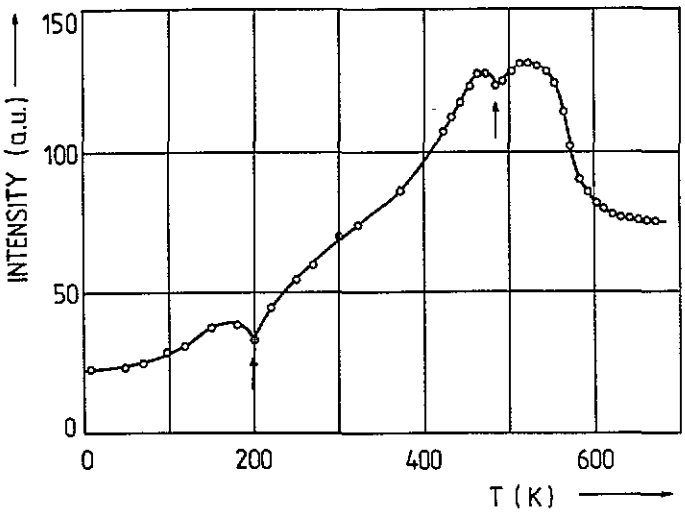

Figure 12. Variation in the constant-frequency (52 cm^{-1}) light intensity scattered with increasing temperature by the PLZT 2/92/8 ceramics. The rate of temperature variation was 8 K min^{-1}.

Moreover, the observed $P_r(T)$ characteristics deviate markedly from those resulting from phenomenological theory for PZT solid solutions [22], especially in the part corresponding to the $F_{R(HT)}$–$F_{R(LT)}$ phase transition. The observed differences in the properties of low-temperature F_R phase may result mainly from its coexistence with the A_O phase and, as discussed above, the two ways of compensating the depolarization field energy and consequently from different reactions of such compensated ferroelectric domains to the external factors. This may reasonably be taken to be the principal cause of the observed differences in the properties of the F_R phase in its high- and low-temperature parts.

A qualitative interpretation model in many respects similar to that presented here was given in our earlier papers [11, 17, 19] to explain the specific features of low-frequency dielectric dispersion and TSDC characteristics, observed in the paraelectric phase of PLZT $x/95/5$ and Nb-doped PZT 95/5 ceramics. In the present paper, it is shown that processes of a similar nature play an even more important role in the broadening of the F_R–A_O phase transition and especially in the stabilization of the remaining ferroelectric domains in the antiferroelectric matrix.

References

[1] Dungan R, Barnett H M and Stark A H 1962 *J. Am. Ceram. Soc.* **45** 382
[2] Berlincourt D, Krueger H H A and Jaffe B 1964 *J. Phys. Chem. Solids* **25** 659
[3] Troccaz M, Eyround L, Fettiveau Y and Gonnard P 1973 *C.R. Acad. Sci. Paris* B **276** 547
[4] Clarke R and Glazer A M 1974 *J. Phys. C: Solid State Phys.* **7** 2147
[5] Handerek J and Ujma Z 1977 *Acta Phys. Pol.* A **51** 87
[6] Morozov E M 1977 *Fiz. Tverd. Tela* **7** 42
[7] Whatmore R W, Clarke R and Glazer A M 1978 *J. Phys. C: Solid State Phys.* **11** 3089
[8] Handerek J, Kwapulinski J, Pawełczyk and Ujma Z 1985 *Phase Trans.* **6** 35
[9] Handerek J, Kwapulinski J, Ujma Z and Roleder K 1988 *Ferroelectrics* **81** 253
[10] Haertling G H and Land C E 1971 *J. Am. Ceram. Soc.* **54** 1
[11] Handerek J, Ujma Z, Carabatos-Nedelec C, Kugel G E, Dmytrow D and El-Harrad I 1993 *J. Appl. Phys.* **73** 367

[12] Bauerle D, Holzapfel W B, Pinczuk A and Yacoby Y 1977 *Phys. Status Solidi* b **83** 99
[13] Fritz I J and Keck J D 1978 *J. Phys. Chem. Solids* **39** 1163
[14] Barnett H M 1962 *J. Appl. Phys.* **33** 1606
[15] Michel C, Moreau J M, Achenbach G D, Gerson R and Janes Y J 1969 *Solid State Commun.* **7** 865
[16] Randall C A, Matsko M G, Cao W and Bhalla A S 1993 *Solid State Commun.* **85** 193
[17] Hafid M, Kugel G E, Handerek J and Ujma Z 1992 *Ferroelectrics* **135** 101
[18] Carabatos-Nedelec C, El Harrad I, Handerek J, Brehard F and Wyncke B 1992 *Ferroelectrics* **125** 483
[19] Hafid M, Handerek J, Kugel G E and Fontana M D 1992 *Ferroelectrics* **125** 477
[20] El Harrad I, Carabatos-Nedelec C, Handerek J, Ujma Z and Dmytrow D 1994 *J. Raman Spectrosc.* at press
[21] Roleder K, Kugel G E, Fontana M D, Handerek J, Lahlou S and Carabatos-Nedelec C 1989 *J. Phys.: Condens. Matter* **1** 2257
[22] Haun M J, Halemane R T, Newnham R E and Cross L E 1985 *Japan. J. Appl. Phys.* **24** 209
[23] Haertling G H 1991 *Ceramic Materials for Electronics* (New York: Buchanan) ch 3